


Article

A Novel Electrode Front-End Face Design to Improve Geometric Accuracy in Electrical Discharge Machining Process

Shih-Ming Wang ¹, Jin-Kai Peng ², Hariyanto Gunawan ^{2,3,*} , Ren-Qi Tu ^{2,3} and Shean-Juinn Chiou ¹

¹ Department of Mechanical Engineering, National Chung Hsing University, Taichung 40227, Taiwan; shihmingbear@nchu.edu.tw (S.-M.W.); sjchiou@dragon.nchu.edu.tw (S.-J.C.)

² Department of Mechanical Engineering, Chung Yuan Christian University, Taoyuan 320314, Taiwan; g10873009@cycu.edu.tw (J.-K.P.); g10902308@cycu.edu.tw (R.-Q.T.)

³ R&D Center for Smart Manufacturing, Chung Yuan Christian University, Taoyuan 320314, Taiwan

* Correspondence: harrywey@cycu.edu.tw

Abstract: Electrical discharge machining (EDM) is one of the important machining processes to produce mold components. When using the EDM process, surface quality, processing time, accuracy, and electrode cost must be considered. The electrode wear is the main factor that causes error on the geometric accuracy, especially the workpiece corner. Therefore, this study proposes a novel electrode design to improve the geometric accuracy for the EDM process. Firstly, the effect of discharge current, electrode diameter, and depth of cut on the electrode wear and workpiece corner were investigated. Multiple regression and analysis of variant were used to analyze the experiment data. The electrode end-face design with compensation rule and algorithm was established based on the data analysis and error value. Furthermore, a compensated electrode end-face design system with human machine interface, which has a procedure guiding function, was developed. The system can design the electrode end-face for minimizing workpiece corner error and improve geometric accuracy. Finally, cutting experiments were conducted to verify the proposed method, and the results show that the proposed method can effectively enhance the geometric accuracy by around 22~37%.

Keywords: electrical discharge machining; electrode end-face design; geometric accuracy; workpiece corner error



Citation: Wang, S.-M.; Peng, J.-K.; Gunawan, H.; Tu, R.-Q.; Chiou, S.-J. A Novel Electrode Front-End Face Design to Improve Geometric Accuracy in Electrical Discharge Machining Process. *Metals* **2023**, *13*, 1122. <https://doi.org/10.3390/met13061122>

Academic Editor: Shoujin Sun

Received: 13 May 2023

Revised: 10 June 2023

Accepted: 13 June 2023

Published: 15 June 2023



Copyright: © 2023 by the authors. Licensee MDPI, Basel, Switzerland. This article is an open access article distributed under the terms and conditions of the Creative Commons Attribution (CC BY) license (<https://creativecommons.org/licenses/by/4.0/>).

1. Introduction

In recent years, the demand for high-quality high-precision products such as electronic devices, automotive components, medical devices, etc., has significantly increased. The injection molding process is usually used to produce these plastic products. To obtain high quality and precise products depends on the mold. Therefore, it is a challenge to make a high quality and high accuracy mold. Special material with high hardness is generally chosen for the mold material to obtain wear resistance and abrasion resistance.

Electrical discharge machining (EDM) is a type of non-traditional machining process, commonly used in the machining of hardness materials. EDM can work on any conductive material regardless of its hardness and generates no internal stress in the workpiece due to the fact that the electrode does not make contact with the workpiece [1–3]. EDM is a process that removes material by generating high thermal energy through repeated sparking that ionizes the dielectric fluid present in the gap between the tool electrode and workpiece, creating an identical copy of the electrode profile on the workpiece [4,5]. The discharge intensity produces a plasma channel that acts as a strong source of heat, causing localized heating. The plasma channel causes the particles from the workpiece to melt and vaporize, which is aided by a series of electrical discharges that can increase the temperature up to 12,000 °C [6,7]. The debris is removed from the workpiece by the dielectric liquid, which is directed onto the cutting zone [8,9]. The success of the EDM process is influenced by both machine-related and user-defined factors such as discharge

current, breakdown voltage, gap voltage, pulse-on time (T_{on})/off time (T_{off}), machining time, duty cycle, dielectric pressure, etc. The efficiency of the EDM process can be evaluated based on various parameters, including material removal rate (MRR), surface roughness (SR), tool wear rate (TWR), surface integrity, and dimensional accuracy of the finished product [10]. Enhancing material removal rate (MRR) and reducing tool wear rate (TWR) are crucial for EDM to compete with conventional machining processes on economic grounds. Decreasing TWR and minimizing tool wear have a positive impact on machining precision since slower changes to the electrode's profile and geometry maintain high precision levels. However, EDM is a multi-parameter process, controlling the occurrence of sparks during the machining process is a challenge, and it is difficult to achieve precise cutting dimensions in all orientations [11].

Several studies examined the impact of process parameters on dimensional error during EDM of various materials. Bhosle et al. [12] used grey relational analysis (GRA) to optimize parameters for micro-EDM of Inconel 600 using EDM oil as a dielectric. They investigated five machine factors, including capacitance, voltage, pulse-on/off time, and feed rate, and found that capacitance was the most influential factor affecting error magnitude. Cyril et al. [13] conducted micro-electro-discharge drilling on stainless steel 316 L with varying amounts of different additives, such as Al, graphite, and silicon carbide (SiC), added to the dielectric liquid DCO 1000i EDM oil. They reported that overcut (OC) increased with the addition of more additives due to significant discharging and that OC could be reduced in the absence of additives in the dielectric medium. The high value of the overcut was attributed to the large dispersion of arcing between the work surface and electrode [14]. Zainal et al. [15] investigated the effect of process parameters, including T_{on} , T_{off} , servo voltage, and peak current, on the dimensional accuracy of Ti6Al4V during EDM using copper–tungsten (Cu–W) as a tool material and conventional EDM oil as the dielectric liquid. They employed a full factorial experimental design and determined the optimum values of the process parameters using a mathematical model. The results show a significant reduction in overcut after setting the parameters at the predicted optimum values.

Anand et al. [16] attempted to optimize the EDM process in terms of environmental sustainability, taking into account factors such as relative electrode wear ratio, energy consumption, and process time. Four control factors were selected to minimize output responses: peak current, pulse duration, flushing pressure, and dielectric level. The Taguchi method was utilized to optimize these parameters, and it was found that the output responses were primarily influenced by peak current and dielectric level, while pulse duration had the least impact. Ahmed et al. [17] studied dimensional errors in both radial and axial orientation during EDM of Ti6Al4V, using four different electrode materials (aluminum (Al), brass (Br), copper (Cu), and graphite (Gr)) under kerosene dielectric. They considered three input factors: tool polarity, discharge current, and pulse time ratio, and found that the selection of negative polarity and Cu electrode significantly decreased geometric errors.

The electrode material also influences the tool wear rate. Mandal et al. [18] utilized an electrolytic copper electrode and C40 workpiece. They varied the duration of pulse-on time from 23 to 506 μ s, pulse-off time from 23 to 248 μ s, and discharge current from 4–16 A. The experiment results show that increasing discharge current and pulse-on time results in higher electrode consumption, whereas increasing pulse-off time results in lower electrode consumption. Muthuramalingam et al. [19,20] investigated the influence of tool electrode material on the workpiece erosion. They explored the effects of using copper, brass, and tungsten carbide electrode materials on the erosion of both the workpiece and the tool. The experiment results indicate that using a copper tool results in a higher material removal rate, while tungsten carbide tools yield better surface finishes after the machining process. Furthermore, the use of tungsten carbide increases the surface hardness of the workpiece, whereas using a brass tool electrode leads to a decrease in surface hardness due to the formation of a layer on the machined surface. Prasanna et al. [21] compared the performance of different electrode materials such as Cu and alumina–titanium-oxide-

coated Cu under conventional EDM oil, considering overcut as a response attribute. They found that the coating on the Cu electrode reduces overcut by 62.5%. Similarly, Karmiris-Obratanki et al. [22] carried out a comparative investigation involving the utilization of copper and graphite electrodes for machining of Ti6Al4V ELI. They employed analysis of variance (ANOVA) to assess the significance of each process parameter on the MRR, TWR, and surface quality when different type of electrodes were employed. Ishfaq et al. [23] investigated three types of electrode material, namely, copper, graphite, and tungsten carbide, which are metals, nonmetals, and ceramics, respectively, and they were compared for their performance in relation to different parameters. The results indicate that the axial errors are 2.5 times less than lateral dimensional errors. Graphite electrodes are found to be the most promising for reducing laterals errors, while copper electrodes are found to be the best for reducing axial errors. The mean axial error obtained with a copper electrode is 80.9% and 47.6% lower than that achieved with graphite and tungsten carbide, respectively.

To reduce the dimensional errors in EDM, researchers attempted to modify the electrode geometry. They employed electrodes with a certain relief angle and observed a reduction in the value of overcut [24]. Liang et al. [25] proposed a self-repair method and a profile error compensation method for tool electrode wear to improve processing accuracy. The self-repair method controls the rotation motion of the tool electrode, while the profile error compensation method modifies the Z coordinate of the tool electrode. Lo et al. [26] employed enveloped theory to present an electrode compensation technique that aim to eliminate deviation errors. These techniques are based on kinematic geometry, which integrates the motion path of tool bodies and constraints to trace out a family of electrode curves. By using a compensation electrode in the orbiting process, the deviation error between the orbiting and objective profiles can be eliminated, ensuring that the generated orbiting profile conforms to the objective profile. Experimental results show that the compensation method is effective in eliminating profile deviation and improving the EDM profile's precision. Richard et al. [27] examined the relationship between electrode profile and tool path trajectory, theoretically and experimentally. A cylindrical electrode with a trajectory in full material leads to a conically self-shaped profile, while a zigzag pocketing trajectory created a more complex self-shaped profile linked to the tool path overlap, steepness, and EDM gap. Pei et al. [28] proposed a truncated conic tool-end. An analytical model was developed that links the truncated conic shape to fix-length compensation parameters, which is then used to determine machining parameters corresponding to a preset milling depth. Yu et al. [29] proposed a compensation technique called the combination of the linear compensation and the uniform wear method (CLU), which merges the linear compensation method (LCM) and the uniform wear method (UWM). The experiment results indicate an improvement in the machining efficiency and reducing the tool wear.

In the past, the researchers studied the electrode wear and circular corner error in EDM, but there were only improvements in the machining depth but not the circular corners. Although the installation of a high-speed spindle and front-end face cutting and trimming of the electrode could improve the circular corner of the workpiece, repairing the electrode takes time and may cause burrs and affect the accuracy. Therefore, this study proposed a new method to enhance workpiece corner accuracy by designing an electrode front-end face. The first examined the impact of cylindrical electrodes parameters on the curvature of workpiece corners. Based on the previous research mention above, the discharge current has a significant impact on the tool wear rate, so in this study discharge current was chosen. Additionally, two other parameters such as electrode diameter and depth of cut were also chosen parameters. The experiment with the variation in these three parameters was conducted, while other machining parameters were fixed. Furthermore, multiple regression and analysis of variant were performed to establish the prediction regression model and investigate the main effect and interaction effect of each parameter on the workpiece corner. The second, focused on electrode front-end shape design. A design rule was created according to experimental design, planning, and data analysis. Furthermore, the rules of these two parts were combined into an integrated algorithm to

design an electrode tool that obtained a smaller workpiece corner error. In addition, a systematic computer-aided design system with a user-friendly human–machine interface that can design electrode front-end shapes, and predict the workpiece corner error and processing depth to obtain smaller workpiece corner error was developed using Visual C# programming language.

2. Methodology

In EDM, the electrode wear and machining efficiency are two problems to be solved [30]. A seriously worn electrode would directly affect depth and workpiece shape accuracy. Therefore, it is necessary to understand the effect of machining parameters on the electrode wear and workpiece shape accuracy, and compensate the electrode wear incurred during machining.

The parameters used in EDM are dependent on the processing conditions, and these conditions have an impact on various aspects such as the electrode wear rate, material removal rate, spark gap, and dimensional accuracy of the final product. The aim of this research was to develop a computer-aided design system that can design an electrode tool shape to reduce the workpiece corner error. Therefore, the overall experiment was essentially divided into three parts.

The first part investigated the effect of cylindrical electrode wear on the accuracy of the whole workpiece. The experiments with different discharge current, electrode diameter, and depth of cut setting were conducted, then the radius of the workpiece corner were measured. The obtained data were analyzed using the commercial software IBM SPSS statistic to optimize the parameters in order to obtain a smaller workpiece corner error, and then an algorithm was created according to multiple regression. Moreover, the effect and influence of various electrode diameters, discharge current, and depth of cut on the workpiece corner error were investigated and explored.

In the second part, the workpiece corner was transformed into volume or a cross-sectional area, and three different electrode front-end shapes were designed. The effect of the electrode front-end volume, width-to-height ratio of the face-end shape, and the machining time on the accuracy of the workpiece corner were investigated.

The third part developed a user-friendly human–machine interface that can predict the workpiece corner error, and design the electrode front-end shape (width and height) as well as the machining depth for reducing workpiece corner error. The evaluation of the proposed method was also carried out to verify the improvement in workpiece corner accuracy.

2.1. Experiment Condition and Equipment

Figure 1 shows the schematic diagram of the experiment. CHMER die sinker EDM model CM323C manufactured by Ching Hung Machinery and Electric Industrial Co., Ltd., Taichung city, Taiwan with resolution of 0.001 mm, discharge current 0–48 A, pulse-on/off time range of 1–2400 μ s, open circuit voltage 120–280 V, and maximum machining speed of 350 mm³/min was used in the experiment. Copper is typical and widely used in EDM due to good machinability, thermal and electric conductivity, the fact it is not prone to arcing, and generates less wear [31]. Meanwhile, the SKD11 tool steel with dimension of size 70 × 50 × 40 mm (length × width × height) was used as workpiece material. SKD11 tool steel is high-carbon high-chromium alloy steel with extremely high hardness (up to HRC58–62), and good strength and wear resistance. It is commonly used in various cold working molds, such as punching dies, cutting dies, deep drawing dies, punching heads, etc. In this experiment, electrode copper cylinders with diameters of 10, 12, and 15 mm were used. Three different depths of cut of 3, 6, and 8 mm were chosen. Regarding machining parameters, three level discharge currents of 10, 16, and 20 A were chosen, as shown in Table 1. The rest of the parameters were held constant according to the CHMER EDM manufacturer recommendations such as pulse-on time 50 μ s, pulse-off time 100 μ s, open circuit voltage 240 V, working time 0.4 s, servo code 706, open gap voltage 140 V, and electrode jump height 1 mm. The rounded corner of the workpiece was measured using

2.5D video measurement system VMS-2515 with resolution of 0.5 μm , X-, Y-, Z-motion resolution of 1 μm , produced by Licheng Optoelectronics Technology Co., Ltd., Guangdong city, China. Each experiment result was measured three times, then the average value was calculated.

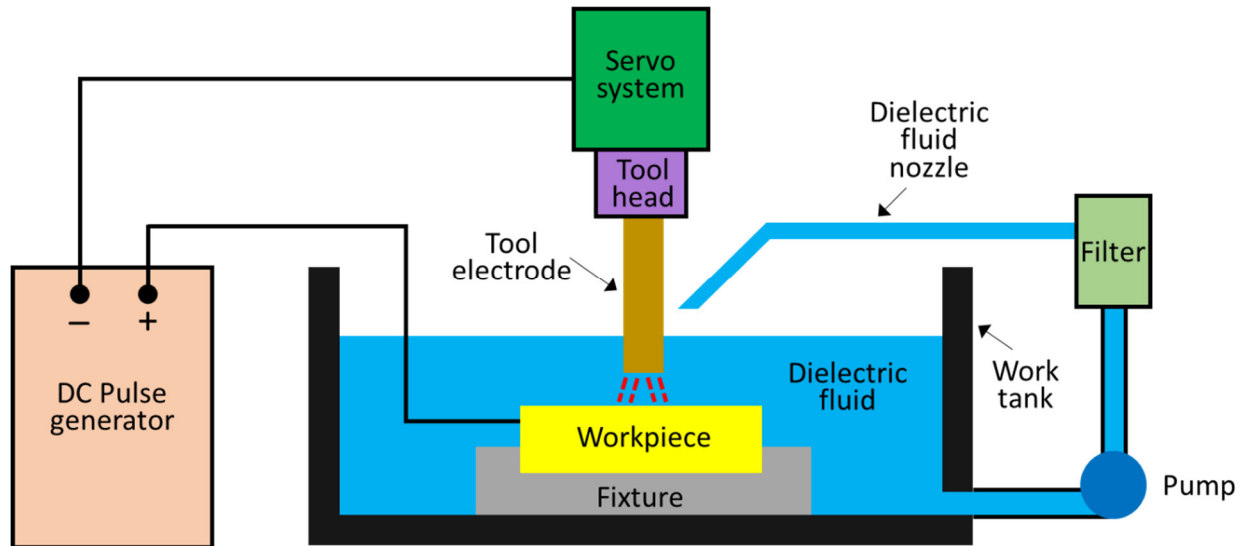


Figure 1. Schematic diagram of experiment.

Table 1. EDM process parameter and their levels.

Level	Electrode Diameter (mm)	Discharge Current (A)	Depth of Cut (mm)
1	10	10	3
2	12	16	6
3	15	20	8

In order to conduct an experiment effectively, the statistical design of experiments (DOE) was used, so that appropriate data could be collected and analyzed with statistical techniques, resulting in valid and objective conclusions. The full factorial design was used to determine the number of experiments for obtaining an adequate model of responses. Therefore, with 3 parameters and 3 levels, and each level of each parameter being tested 3 times, the total number of experiment was 81.

The software IBM SPSS statistics 26 and Minitab were utilized to analyze the workpiece corner radius data from the experiments. The multiple regression analysis was used to investigate the relationship between machining parameters, electrode wear, and workpiece corner. Multiple regression, such as simple linear regression, explores the relationship between independent variable (X) and dependent variable (Y) and establishes a regression model to predict the variable (Y) of user demand. The difference between these two is that multiple linear regression uses more than two independent variables (X) to predict the dependent variable (Y). In this study, the dependent variable (Y) was the workpiece corner radius, while the independent variable was the electrode diameter (X_1), discharge current (X_2), and depth of cut (X_3). The multiple linear equation is shown in Equation (1).

$$Y = \beta_0 + \beta_1 X_1 + \beta_2 X_2 + \beta_3 X_3 \quad (1)$$

where β_0 is the response variable at the base level; β_1 , β_2 , and β_3 are the regression coefficient associated with electrode diameter, discharge current, and depth of cut, respectively.

In order to evaluate the accuracy of the regression model, the coefficient R-square was analyzed. If the R-square value is greater than 0.75, it suggests that the model has a good fit, while a value less than 0.75 indicates a problematic model fit and this regression model

should not be used. Although a higher R-square value can make the model more accurate, there may be some independent variables (X) that are not related to the dependent variable (Y), and, therefore, will not improve the model fit and prediction accuracy. Consequently, most scholars prefer to use the adjusted R-square to avoid poor predictions by the regression model [32]. Furthermore, analysis of variance (ANOVA) and the significance test (F test, t -test) of the regression model were conducted. To ensure the accuracy, a confidence interval of 95% should be achieved and the p -value should be less than 0.05. If the data do not follow a normal distribution, the p -value is greater than 0.05, resulting in the poor prediction accuracy of the model.

2.2. Electrode Front-End Face Design

During the EDM process, the electrode wears, starting from the sharp corner, then followed by the edge, and flat. The front-end corner and edge of the electrode become rounded due to wear, as shown in Figure 2a, resulting in rounded corners in the workpiece. Considering that the consumed part of electrode was at the corner, the design of the electrode front-end face used a mirror method according to the shape of the consumed electrode, as shown in Figure 2b. However, it is difficult to machine the sharp corners. Additionally, during the EDM process, sharp areas are easily consumed or deformed when they collide with one other, leading to inaccurate discharge machining depth. Therefore, the sharp corner was modified into a rounded corner or flat shape to increase the contact area, as shown in Figure 3a,b, but the volume of the electrode front-end face remained the same. However, the preparation of the electrode front-end face with a curved surface is time-consuming. Therefore, another electrode front-end face with a rectangle shape was designed, as shown in Figure 3c, which is easy to prepared.

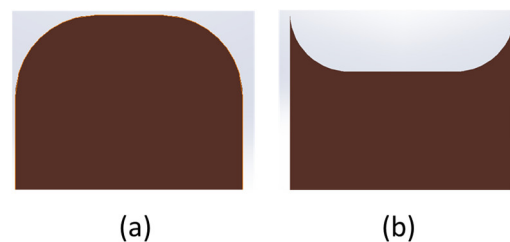


Figure 2. Scheme of (a) electrode with rounded corner caused by wear, (b) design of electrode using mirror of wear.

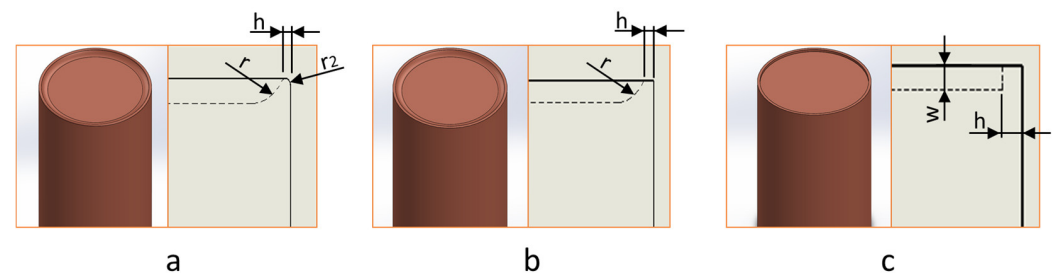


Figure 3. The electrode front-end face design (a) rounded corner, (b) flat, (c) rectangle. (w is height of protrusion, h is width of protrusion, r is radius of inner protrusion, r_2 is radius of outer protrusion).

The volume of the workpiece rounded corner is proportional to the volume of the consumed part of the electrode front-end face. To measure the size of the rounded corner in the workpiece, a cylindrical electrode was used with a fixed depth, and the consumed volume was calculated accordingly. If the machining depth is set to the initial depth of cut (h_0) during the EDM process, the finished workpiece cavity depth is shorter (h_1) due to the electrode wear in front-end face (h), as shown in Figure 4. Therefore, an additional height, which is equal to h value, is required for machining depth compensation to achieve the initial cavity depth after the electrode wear.

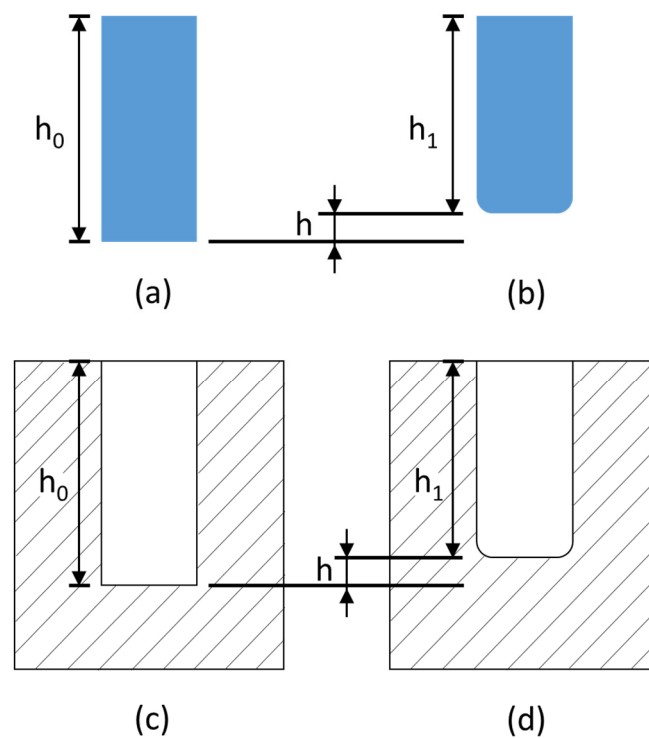


Figure 4. (a) Initial electrode design, (b) electrode shorter due to wear, (c) ideal workpiece cavity, (d) actual workpiece cavity due to electrode wear.

3. Results and Discussion

The experiment results for different machining parameters are shown in Table 2. It is found that using the electrode diameters of 10 and 15 mm, discharge current 10 A, and depth of cut 3 mm produce a workpiece corner radius of 0.303 and 0.441 mm, respectively. With the discharge current and depth of cut held constant, an increase in electrode diameter results in a larger workpiece corner radius. In addition, the workpiece corner radius is found to be 0.4 and 0.882 mm when using an electrode diameter of 10 mm, depth of cut 6 mm, and discharge current of 10 and 20 A, respectively. This indicates that when the electrode diameter and depth of cut are held constant, an increase in the discharge current results in a larger workpiece corner radius. For the electrode diameter of 15 mm, depth of cut of 3, 6, and 8 mm, and using discharge current 16 A, this results in workpiece corner radii of 0.599, 0.705, and 0.805 mm, respectively. If the electrode diameter and discharge current remain constant, increasing the depth of cut leads to a larger workpiece corner radius. Additionally, the workpiece corner radius grows proportionally with the depth of cut. Table 2 shows that as the discharge current increases, the workpiece corner radius increases at a consistent rate for increasing depth of cut.

Table 2. Effect of machining parameters on the workpiece corner.

Electrode Diameter (mm)	Discharge Current (A)	Depth of Cut (mm)	Workpiece Corner Radius (mm)
10	10	3	0.303
10	10	6	0.4
10	10	8	0.518
10	16	3	0.475
10	16	6	0.663
10	16	8	0.801
10	20	3	0.68
10	20	6	0.882

Table 2. Cont.

Electrode Diameter (mm)	Discharge Current (A)	Depth of Cut (mm)	Workpiece Corner Radius (mm)
10	20	8	1.085
12	10	3	0.358
12	10	6	0.444
12	10	8	0.563
12	16	3	0.492
12	16	6	0.661
12	16	8	0.823
12	20	3	0.708
12	20	6	0.915
12	20	8	1.071
15	10	3	0.441
15	10	6	0.512
15	10	8	0.588
15	16	3	0.599
15	16	6	0.705
15	16	8	0.805
15	20	3	0.75
15	20	6	0.969
15	20	8	1.08

3.1. Mathematical Model Analysis

The ANOVA analysis was carried out using data in Table 2, and it shows that the R-square, adjusted R-square, and predicted R-square values are 95.4%, 94.4%, and 92.1%, respectively. To enhance the prediction accuracy of the regression model, two segments of regression were approached. Since the various discharge currents produce a wider range of workpiece corner radii compared to the various electrode diameter or depth of cut, the discharge current parameter was chosen to be divided into two segments. In the experiment, the discharge currents of 10, 16, and 20 A were used. Therefore, the first set was for 10 and 16 A (model 1), and the second set was for 16 and 20 A (model 2). The ANOVA results for workpiece corner radius are presented in Table 3. It can be seen that the R-square, adjusted R-square, and predicted R-square values are 95.7%, 95.1%, and 93.7%, respectively, for model 1, which indicates a slight improvement in the model accuracy. Additionally, the p -value is less than 0.05, which means that the model has a significant prediction ability, and a confidence interval of 95% or more. Meanwhile, the R-square, adjusted R-square, and predicted R-square values for model 2 are 98.1%, 97.9%, and 95.8%, respectively, indicating a better fit of the model. The p -value is less than 0.05 and satisfies the confidence of interval of at least 95%. This suggests that the model has a considerable ability to make predictions. Tables 4 and 5 present the t -test results of each individual regression coefficient for models 1 and 2. From these tables, it is evident that all three input parameters, namely, discharge current, electrode diameter, and depth of cut, have a significant effect on the workpiece corner radius. Based on the data in Tables 4 and 5, the regression equation for models 1 and 2 can be formulated as Equations (2) and (3), respectively:

$$r = (36.167C_D + 13.935D_E + 49.234h_C - 354.671)/1000 \quad (2)$$

$$r = (57.229C_D + 11.338D_E + 65.819h_C - 756.444)/1000 \quad (3)$$

where r is estimated value of workpiece corner radius (mm), C_D is discharge current (A), D_E is electrode diameter (mm), and h_C is depth of cut (mm).

Table 3. ANOVA result for workpiece corner radius.

Source	Sum of Square	DF	Mean Square	F Value	p Value
Model 1					
Regression	559,324.881	3	186,441.627	149.323	0.000
Residual	24,971.619	20	1248.581		
Total	584,296.500	23			
$R^2 = 95.7\%$ $R^2_{adj} = 95.1\%$ $R^2_{pred} = 93.7\%$					
Model 2					
Regression	774,040.695	3	258,013.565	352.784	0.000
Residual	14,627.263	20	731.363		
Total	788,667.958	23			
$R^2 = 98.1\%$ $R^2_{adj} = 97.9\%$ $R^2_{pred} = 95.8\%$					

Table 4. Coefficient value of model 1 for workpiece corner radius.

Independent Variable	Unstandardized Coefficients		Standardized Coefficient	t	Sig
	B	Std. Error	Beta		
(Constant)	−354.671	49.083	-	−7.226	0.000
Discharge current	36.167	2.404	0.695	15.043	0.000
Electrode diameter	13.935	2.789	0.231	4.996	0.000
Depth of cut	49.234	3.510	0.648	14.026	0.000

Table 5. Coefficient value of model 2 for workpiece corner radius.

Independent Variable	Unstandardized Coefficients		Standardized Coefficient	t	Sig
	B	Std. Error	Beta		
(Constant)	−756.444	57.509	-	−13.153	0.000
Discharge current	57.229	2.760	0.631	20.734	0.000
Electrode diameter	11.338	2.135	5.311	5.311	0.000
Depth of cut	65.819	2.687	24.500	24.500	0.000

3.2. Analysis of Electrode Front-End Face Design

To investigate the impact of the proposed three electrode front-end face designs on the radius of the workpiece corner after discharging, the experiment using three different discharge currents of 10, 16, and 20 A was conducted. In addition, an electrode diameter of 10 mm and machining depth of cut of 3 mm were chosen, and the volume and height of the electrode front-end face design remained identical for all designs. The experimental results are shown in Table 6.

Table 6. Workpiece corner radius produced by different discharge currents.

Electrode Design	Workpiece Corner Radius (mm)			Electrode Machining Time (min)		
	10 A	16 A	20 A	10 A	16 A	20 A
Design a	0.241	0.418	0.521	19.966	19.2	20.6
Design b	0.238	0.418	0.543	19.233	19.116	20.783
Design c	0.248	0.408	0.513	4.4	3.933	6.333
Cylinder	0.303	0.475	0.678	-	-	-

As seen in Table 6, when using discharge current of 10 A, the workpiece corner radii for designs a, b, and c are 0.241, 0.238, and 0.248 mm, respectively. The maximum

deviation between the designs is 10 μm . When using discharge current of 16 A, this produced workpiece corner radii of 0.418, 0.418, and 0.408 mm for designs a, b, and c, respectively. The maximum deviation between the designs is also within 10 μm . Meanwhile, for discharge current of 20 A, the workpiece corner radii are 0.521, 0.543, and 0.513 mm for designs a, b, and c, respectively. The maximum deviation between the design is 30 μm . The results of the experiment show that the accuracy of the workpiece corner is almost similar for different electrode front-end face designs when the volume of the electrode front-end face design is maintained at a constant.

Regarding the preparing time of the electrode, designs a and b need a longer time duration due to having curved surfaces that require longer machining time. However, design c has no curved surfaces, so only needs approximately 4 min for the preparation; this means it is 3–5 times faster than preparing the electrode designs a and b. Additionally, the accuracy of the workpiece corner is almost same for all three designs. Therefore, subsequent experiments were carried out using electrode design c.

3.3. Analysis of Electrode Front-End Face Volume Design

The experimental results show that when the discharge current is set to 10, 16, and 20 A, and the machining depth is 3 mm, the circular pit defect is found in on the workpiece surface as shown in the lower right corner of Figure 5. This is because the protrusion volume of the electrode front-end face has not yet been fully consumed, so the designed volume of protrusion should be reduced to avoid the generation of circular pits, which lead to poor accuracy of the workpiece bottom surface. The protrusion volume of the electrode front-end face was designed based on the size of radius of cylinder electrode wear. The cross-section area to be designed could be obtained by subtracting the area of the quadrant circle from the area of the square as demonstrated in Equation (4):

$$A = r^2 - \frac{\pi r^2}{4} \quad (4)$$

where A is the cross-section area of the workpiece corner (mm^2), and r is the workpiece corner radius.

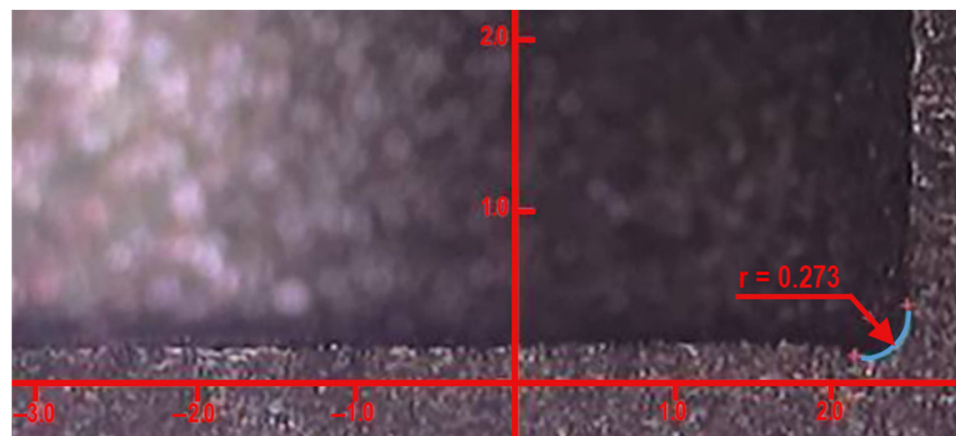


Figure 5. Circular pit defect on bottom surface of workpiece.

Furthermore, the cross-section area was multiplied by the electrode perimeter $2\pi R$, but the perimeter needed to be determined in the middle of the cross-section area, so it was changed to $2\pi\left(\frac{\varnothing}{2} - \frac{\sqrt{\pi r^2/4}}{2}\right)$. Finally, the protrusion volume of the electrode front-end face was reduced by a certain percentage. The formula is shown as Equation (5).

$$V = \left(r^2 - \frac{\pi r^2}{4}\right) \times \pi \times \left(\varnothing - \sqrt{\frac{\pi r^2}{4}}\right) \times V_p \quad (5)$$

where V is electrode protrusion volume, \varnothing is diameter of electrode (mm), and V_p is the percentage of protrusion volume.

Since electrode design c was chosen, the width (w) and height (h) of the protrusion, as shown in Figure 3c, influenced the accuracy of the workpiece corner radius. Therefore, the impact of $w:h$ ratio on the workpiece corner radius was investigated. Table 7 shows the experiment results for workpiece corner radii with different $w:h$ ratio, percentage volume, and depth of cut. The electrode diameter of 10 mm was used for the experiment.

Table 7. Workpiece corner radii for different discharge current, V_p , depth of cut, $w:h$ ratio.

Depth of Cut (mm)	$w:h$	V_p (%)	Workpiece Corner Radius (mm)		
			10 A	16 A	20 A
3	1:1	100	0.248	0.407	0.513
3	1:1	50	0.273	0.401	0.527
3	2:1	50	0.264	0.413	0.512
6	1:1	100	0.291	0.419	0.523
6	1:1	50	0.338	0.545	0.594
6	2:1	50	0.338	0.544	0.595
8	1:1	100	0.295	0.415	0.531
8	1:1	50	0.399	0.580	0.630
8	2:1	50	0.402	0.586	0.631

According to the experimental results, the circular pit defects are found under the conditions of discharge current 10 A, depth of cut 3 mm, and a percentage volume (V_p %) between 100% and 60%. However, under the condition of V_p 50%, no circular pit defects are observed. The workpiece corner radii under V_p 100% and 50% are 0.248 and 0.265 mm, respectively. The difference of 17 μm can be neglected for the general precision requirement of the workpiece corner. The workpiece corner radii are measured to be 0.273 and 0.264 mm when the $w:h$ ratio is 1:1 and 2:1, respectively, and V_p 50%. As seen, the maximum different is 9 μm , indicating the change in $w:h$ ratio has no significant effect on the general precision requirement of the workpiece corner. For a discharge current of 16 A and depth of cut of 3 mm, the circular pit defect is found under V_p 100%, while no circular pits are observed under V_p 50%. When the $w:h$ ratio is changed from 1:1 to 2:1, the workpiece corner radii are 0.401 and 0.413 mm, respectively. Similarly, when the discharge current of 20 A and depth of cut of 3 mm are used, the circular pit defect is only found under V_p 100%. The workpiece corner radii are 0.527 and 0.512 mm for $w:h$ ratio of 1:1 and 2:1, respectively.

When the discharge currents of 10, 16, and 20 A, and machining depth of 6 mm are used, the experiment results show that there are no circular pit defects found under conditions of V_p 100% and 50%. As seen in Table 7, the workpiece corner radii deviations between V_p 100% and 50% for discharge currents 10, 16, and 20 A are 47, 126, and 71 μm , respectively. This deviation value might have a significant impact on the precision of the workpiece corner. On the other hand, modifying the $w:h$ ratio results in a small variation of 1 μm in the workpiece corner radii for different discharge currents, which can be neglected. Based on the experiment, it is observed that a smaller V_p leads to a larger radius of the workpiece corner. Additionally, the precision of the workpiece corner radius is superior when the V_p is 100% compared to when it is 50%. A similar trend is exhibited when the machining depth is set to 8 mm. The circular pit defects do not occur for the V_p 100% and 50% conditions. However, there is a significant difference in workpiece corner radii deviation between V_p 100% and 50% for discharge currents 10, 16, and 20 A, which are 104, 165, and 99 μm , respectively. This difference could have a significant impact on the precision of the workpiece corner. In contrast, changing the $w:h$ ratio leads to minor differences in the workpiece corner radii when using different discharge currents, which are insignificant. It can be concluded that $w:h$ ratio has little effect on the workpiece corner accuracy at

different machining depths. Meanwhile, when the V_p is 100% and the machining depth is 6 or 8 mm, the workpiece corner radius can be maintained at the same size as the corner radius at a depth of 3 mm. However, the corner radius becomes larger with increasing depth. Table 8 exhibits the other percentage of V_p for various discharge currents and depth of cut.

Table 8. Workpiece corner radii for various V_p , discharge current, depth of cut, constant electrode diameter 10 mm, and w:h = 1:1.

V_p (%)	Workpiece Corner Radius (mm)					
	Discharge Current	Circular Pit	Discharge Current	Circular Pit	Discharge Current	Circular Pit
	10 A	Defects	16 A	Defects	20 A	Defects
Depth of cut = 3 mm						
50	0.273	No	0.401	No	0.527	No
60	0.257	Yes	–	–	–	–
80	0.249	Yes	–	–	–	–
85	–	–	0.410	No	–	–
90	–	–	–	–	0.511	No
100	0.248	Yes	0.407	Yes	0.513	Yes
Depth of cut = 6 mm						
50	0.338	No	0.544	No	0.594	No
100	0.291	No	0.545	No	0.523	No
Depth of cut = 8 mm						
50	0.399	No	0.580	No	0.630	No
100	0.295	No	0.415	No	0.531	No

According to the experimental results, a not-uniform surface is found on the workpiece surface with a machining depth of 3 mm, which is due to the electrode front-end protrusion volume not being completely consumed. As is known, during the electrode wear process, the corner is consumed into rounded corners first, and the radius of the rounded corner does not increase linearly until reaching a consumption balance. Therefore, at a machining depth of 3 mm, which is between unbalance and balance, the volume of the electrode front-end protrusion needs to be reduced to 50%, 85%, and 90% for discharge currents of 10, 16, and 20 A, respectively. However, at machining depths of 6 and 8 mm, the electrode front-end protrusion volume can be set to 100%.

Figure 6 shows the conversion of the electrode front-end face volume into a cross-sectional area with protrusion volume 100%. As seen in Figure 6, when the protrusion percentage is 100%, machining depth 3 mm, and discharge current 10 A, the conversion from protrusion volume into protrusion cross-sectional area is 0.0193 mm². Meanwhile, the protrusion cross-sectional area is 0.0343 mm² and 0.058 mm² for machining depths of 6 and 8 mm, respectively. However, using 100% protrusion volume at depth of cut 3 mm produces circular pit defect on the workpiece surface. Therefore, the protrusion volume must be reduced to avoid the occurrence of circular pit defects. On the other hand, when 100% of protrusion volume and machining depth of 6 mm are used, the circular pit defects are not found on the workpiece surface. Similarly, when 100% of protrusion volume and machining depth of 8 mm are used, there is no circular pit defect found on the workpiece surface. Figure 6 also shows that a higher discharge current needs a greater protrusion cross-sectional area, which indicates more protrusion volume is needed to compensate for the electrode tool wear. Additionally, the deeper machining depth is also need for a larger protrusion cross-sectional area.

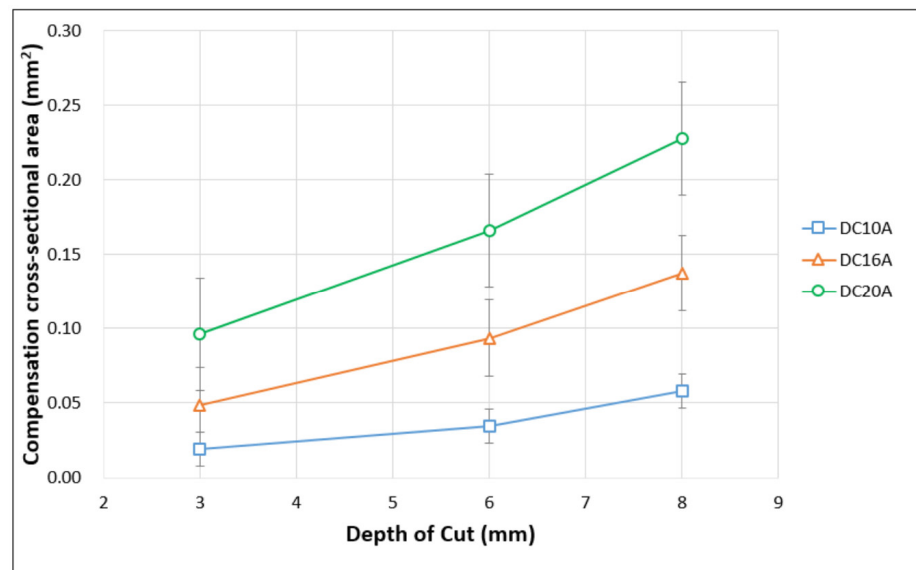


Figure 6. Compensation cross-sectional area for protrusion volume 100%.

Figure 7 shows the conversion of the electrode front-end face volume into cross-sectional area with a reduction in protrusion volume. When 50% of protrusion volume and a machining depth of 3 mm is chosen, the conversion from protrusion volume into a protrusion cross-sectional area is 0.0096 mm^2 , which is smaller compared to that when using 100% protrusion volume, which is 0.0193 mm^2 . Additionally, the circular pit defect is not found on the workpiece surface. When a higher discharge current of 16 A, 85% of protrusion volume, and machining depth of 3 mm are used, the result also shows no circular pit defect on the workpiece surface. Furthermore, when the discharge current of 20 A, 90% of protrusion volume, and machining depth of 3 mm are used, it demonstrates no circular pit defect on the workpiece surface either. Figure 7 also shows similar trends to Figure 6, which is a higher discharge current or larger machining depth needing a larger protrusion cross-sectional area. In addition, the relationship between the cross-sectional area and the machining depth tends toward a linear. By connecting the two points of the cross-sectional area at the depths of 6 and 8 mm with a line, a linear equation can be obtained to predict the cross-sectional area at machining depth of 3 mm and other depths.

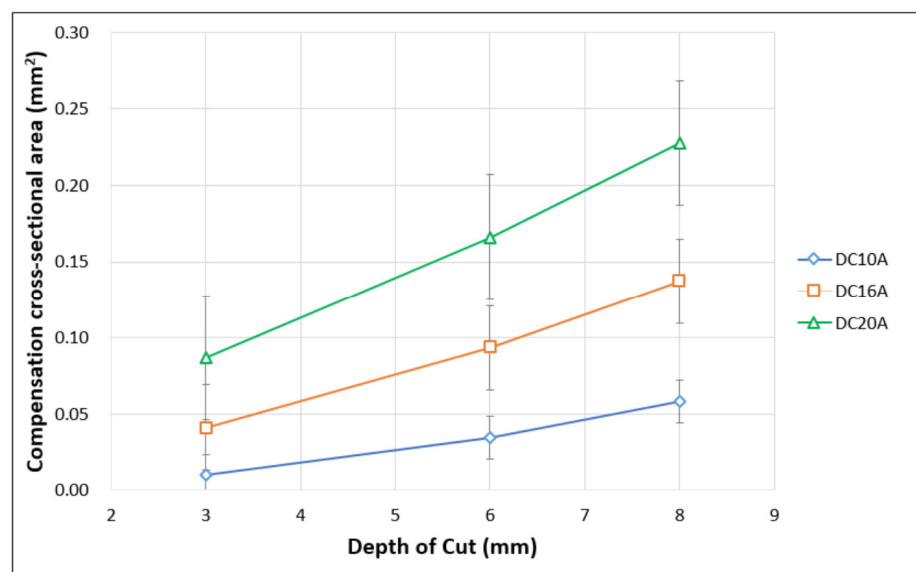


Figure 7. Compensation cross-sectional area for reduced protrusion volume.

The rule to design the electrode without circular fit defects and high accuracy can be summarized into five steps:

- Step 1: Choose the discharge current and electrode size, and input the machining depths of 6 and 8 mm into the regression model of workpiece corners for cylinder electrodes to obtain the workpiece corner radius;
- Step 2: Substitute the obtained workpiece corner radius value in step one into Equation (4) to calculate the cross-sectional area of A_1 and A_2 ;
- Step 3: Substitute the obtained cross-sectional areas into Equation (6) to calculate the slope m . Then, substitute m into Equation (7) to calculate the coefficient b ;

$$m = (A_2 - A_1) / (8 - 6) \quad (6)$$

$$b = A_1 - m \times 6 \quad (7)$$

- Step 4: Substitute the obtained slope and coefficient from step 3 into Equation (8), and input the machining depth (D) to obtain the cross-sectional area of the electrode front-end face design for that machining depth:

$$y = m \times D + b \quad (8)$$

where y is the electrode front-end cross-sectional area (mm^2), D is machining depth (mm);

- Step 5: Substitute the obtained cross-sectional area (y) into Equation (9) to design the width and height using w:h ratio 1:1:

$$w = h = \sqrt{y} \quad (9)$$

where w is the width of the electrode protrusion, h is the height of the electrode protrusion.

3.4. Analysis Correlation of Machining Parameters and Accuracy

Figure 8 shows the main effect of parameters on the workpiece corner radius. It can be seen that the line for discharge current parameter has a steep rise, which indicates the most significant effect on the workpiece corner radius. Meanwhile, the depth of cut also has a significant impact on the workpiece corner radius, which is indicated by the sharp slope. On the other hand, the line for electrode diameter parameter exhibits a slight slope and is close to horizontal, which indicates an insignificant effect on the workpiece corner radius. The contribution of each parameter is 64.7%, 29.4%, and 3.7% for discharge current, depth of cut, and electrode diameter, respectively, as shown in Figure 9. The interaction parameter effect on the workpiece corner radius is displayed in Figure 10. As seen in Figure 10a, the three lines are parallel, which indicates there is no interaction between the discharge current and electrode diameter. Additionally, a trend of increasing is exhibited when the discharge current increases or the electrode diameter is larger. Similarly, there is no interaction between discharge current and depth of cut, and electrode diameter and depth of cut, as shown in Figure 10b,c. In addition, the workpiece corner radius is larger with an increase in discharge current or depth of cut.

Figure 11 shows the experiment results of workpiece corner radius using a cylinder electrode and electrode front-end face design c with a protrusion volume 50%. As is clear in Figure 11, the larger the machining depth, the larger the workpiece corner radius. Similarly, the larger the discharge current, the larger the workpiece corner radius. Furthermore, the proposed electrode front-end face design c results in a smaller workpiece corner radius than the cylinder electrode, indicating an improvement in workpiece accuracy.

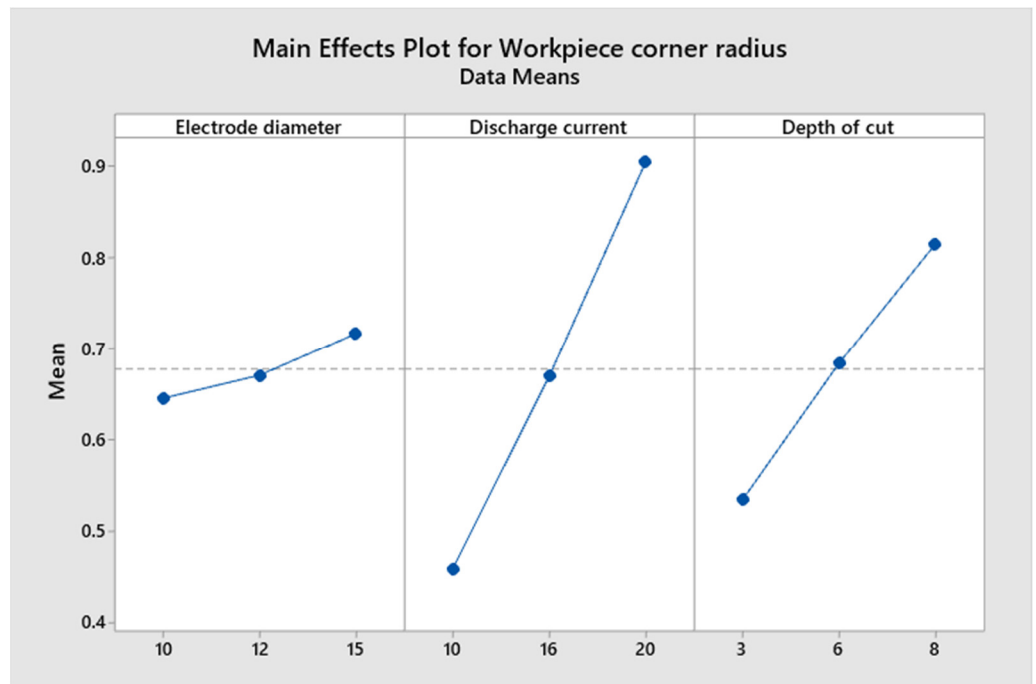


Figure 8. Main effects of machining parameter on workpiece corner radius.

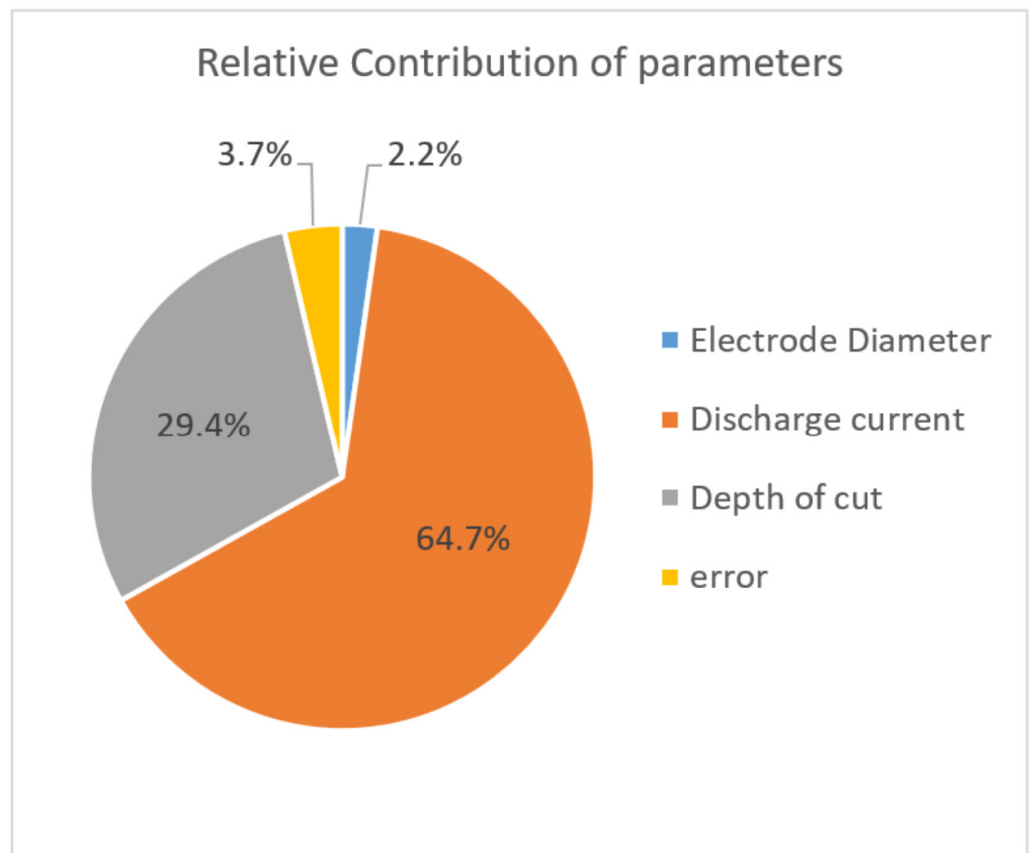


Figure 9. Contribution of each parameter to workpiece corner radius.

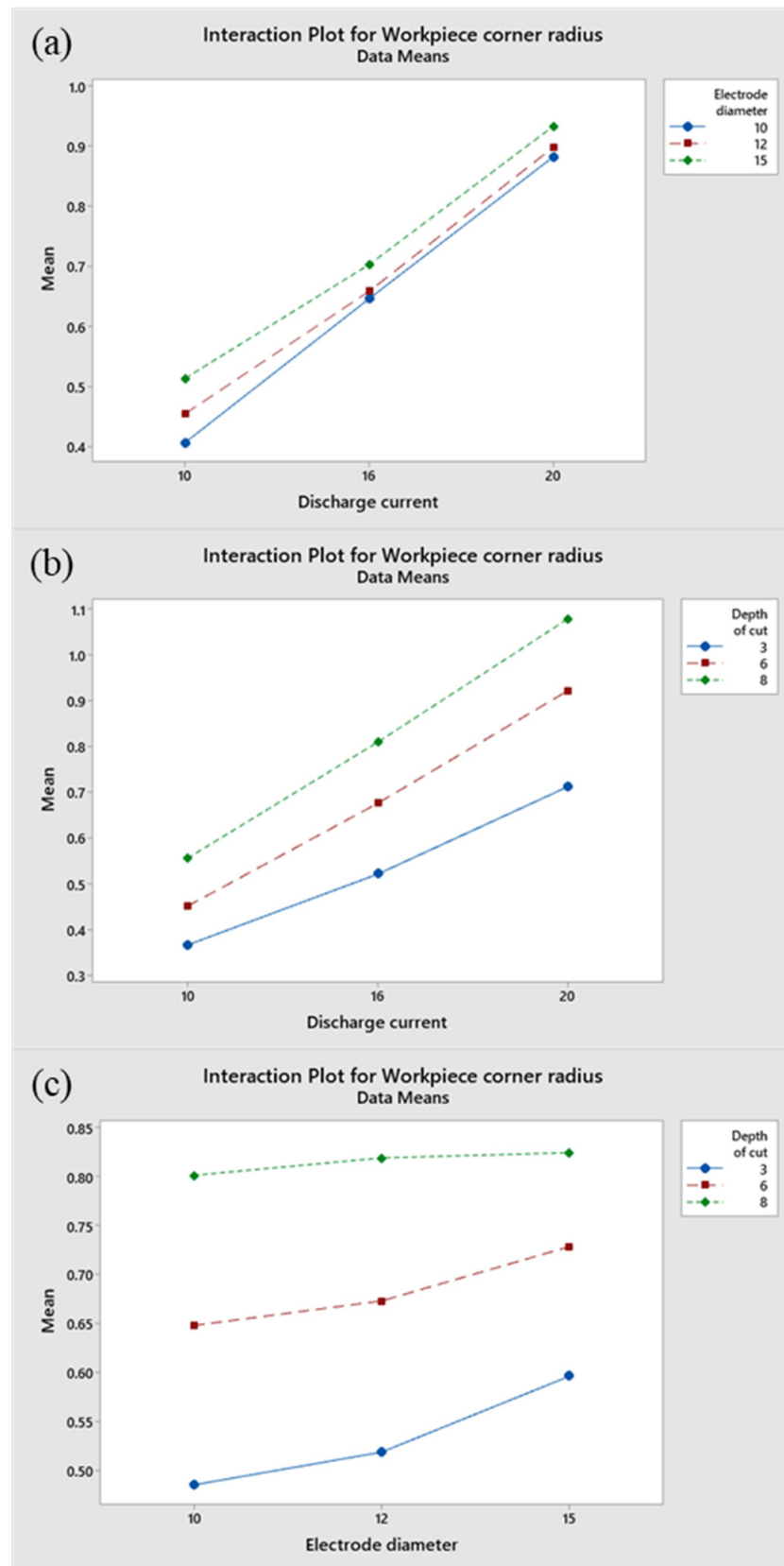


Figure 10. Interaction parameter effects on workpiece corner radius: (a) discharge current vs. electrode diameter, (b) discharge current vs. depth of cut, (c) electrode diameter vs. depth of cut.

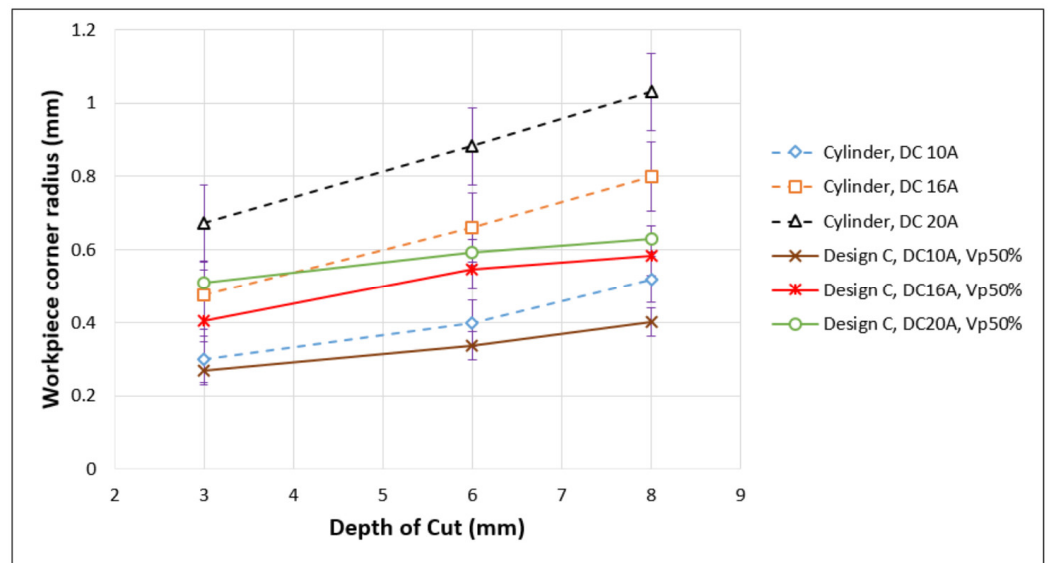


Figure 11. Workpiece corner radius for cylinder electrode and electrode front-end face design c.

Figure 12 shows the experiment results of workpiece corner radius using electrode front-end face design c with a combination of discharge currents, depth of cut, and protrusion volume. The machining depth is 3 mm. For protrusion volume 50%, the discharge current is 10 A; protrusion volume 85% is used for discharge current 16 A; and protrusion volume 90% is used for discharge current 20 A. Meanwhile, the protrusion volume 100% is used for machining depth 6 and 8 mm. It can be seen in Figure 12 that the workpiece corner radii for different depths of cut are quite stable, with deviations of 22, 14, and 18 μm for discharge currents 10, 16, and 20 A, respectively. It is found that the size of the workpiece corner depends on the current, and the accuracy of the workpiece corner is better than that when using a constant protrusion volume of 50%.

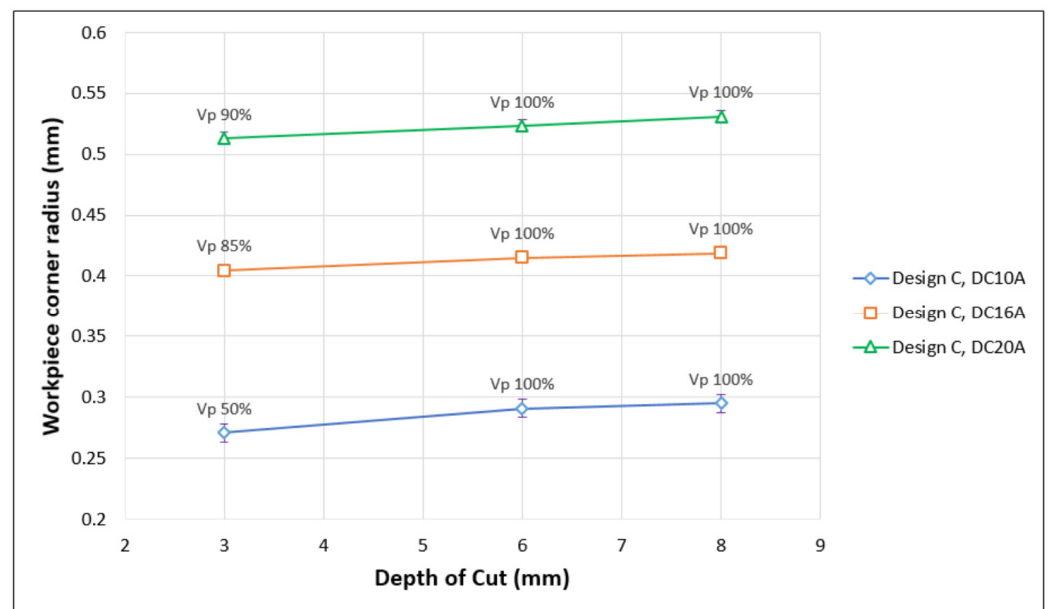


Figure 12. Workpiece corner radii for electrode front-end face design c with different discharge current.

To verify that the discharge current is the most significant factor affecting the workpiece corner as the machining depth increases, an experiment using different pulse-on time was conducted. The experiment used an electrode diameter of 10 mm, discharge current 10 A,

machining depth of 6 mm, and three kinds of pulse-on time: 50, 100, and 200 μs . The experiment results are presented in Table 9. It can be seen that the workpiece corner radii are 0.405, 0.409, and 0.405 mm for pulse-on times of 50, 100, and 200 μs , respectively. The maximum deviation is 4 μm , indicating a small impact on the workpiece corner accuracy.

Table 9. The effect of pulse-on time on workpiece corner radius.

Pulse-On Time (μs)	Workpiece Corner Radius (mm)
50	0.405
100	0.409
200	0.405

4. Human–Machine Interface

The algorithm for designing the front-end face of the electrode is presented in Figure 13. Initially, the user sets certain parameters to estimate the corner radius of the workpiece that will be produced with the cylinder electrode. Then, the volume and size of the front-end face of the electrode are determined using a mirror method. Furthermore, the predicted corner radius of the workpiece produced with the designed front-end face is calculated. Finally, the data on the designed front-end face are stored in an edge computer.

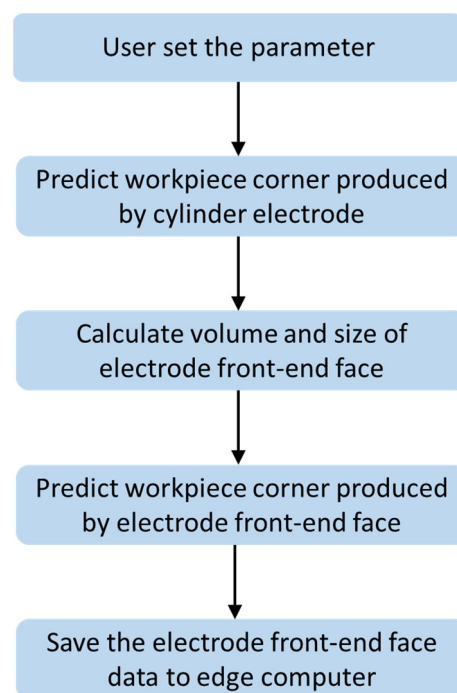


Figure 13. Electrode front-end face design algorithm.

The electrode front-end face design system was created based on the algorithm and was equipped with a human–machine interface (HMI). The HMI was specifically designed to predict the accuracy of workpiece corner, calculate the cross-sectional area, and suggest the size of the electrode protrusion and machining depth. Figure 14 displays the HMI, which was programmed using the C# programming language. The HMI is user-friendly and enables the user to operate the system smoothly. The step by step HMI operation was designed as follows:

1. Input the parameters of electrode material, workpiece material, discharge current, electrode diameter, and machining depth, then choose the calculate button. The system will calculate the workpiece corner radius that will be produced with the cylinder electrode;

2. Choose the compensate button. Then, the compensation page will appear, as shown in Figure 14;
3. Choose the calculate button in the compensation page (Figure 14). The system will calculate the cross-sectional area of the electrode front-end face design, the size of the electrode front-end face design, the machining depth that the machine tool needs to be set, and the predicted workpiece corner radius according to the input parameters;
4. Choose the save button to save all information of input parameters and compensation in CSV file format.

Figure 14. Electrode front-end face design of human–machine interface.

5. Verification Experiments

The verification experiments were carried out to verify the proposed electrode front-end face design method and system. The verification experiment was divided into two parts. The first part verified the design rules for the volume of electrode front-end face protrusions. The workpiece corner radius was verified using an electrode diameter of 15 mm, and machining depths of 3, 6, and 8 mm. The second part was the system verification.

Six experiments were conducted for the first part of the verification. Experiments #1 and #2 consider machining depth, experiments #3 and #4 consider discharge current, and experiments #5 and #6 consider electrode diameter. Table 10 shows the verification experiment parameters.

Table 10. Machining parameters for verification experiment.

Parameter	Value
Pulse-on time T_{on} (μs)	50
Pulse-off time T_{off} (μs)	100
Open-circuit voltage (V)	240
Open gap voltage (V)	140
Servo code	706
Work time	0.4
Electrode jump height (mm)	1
Electrode material	Cu
Workpiece material	SKD11

Figure 15 shows the cross-sectional area using an electrode diameter of 15 mm according to the design rules in Section 3.3. Based on this cross-sectional area, the electrode was designed and used for discharge machining. The experiment results show that the workpiece corner radius is similar to that when using a 10 mm electrode diameter. As shown in Figure 16, when the electrode diameter is 10 mm and discharge current 10 A, the workpiece corner radii are 0.271, 0.291, and 0.295 mm for depth of cut of 3, 6, and 8 mm, respectively. Compared to the electrode diameter of 15 mm with same discharge current of 10 A, the workpiece corner radii are 0.276, 0.288, and 0.295 for depth of cut of 3, 6, and 8 mm, respectively, as shown in Figure 17. It can be seen that the workpiece corner radius deviations between these two electrode diameters are 5, 3, and 0 μm , respectively, and also there are no circular pit defects found. For higher discharge currents of 16 and 20 A, similar trend results are found. As seen in Figures 16 and 17, increasing the discharge current results in a larger workpiece corner radius, however, the workpiece corner does not significantly increase as the machining depth increases.

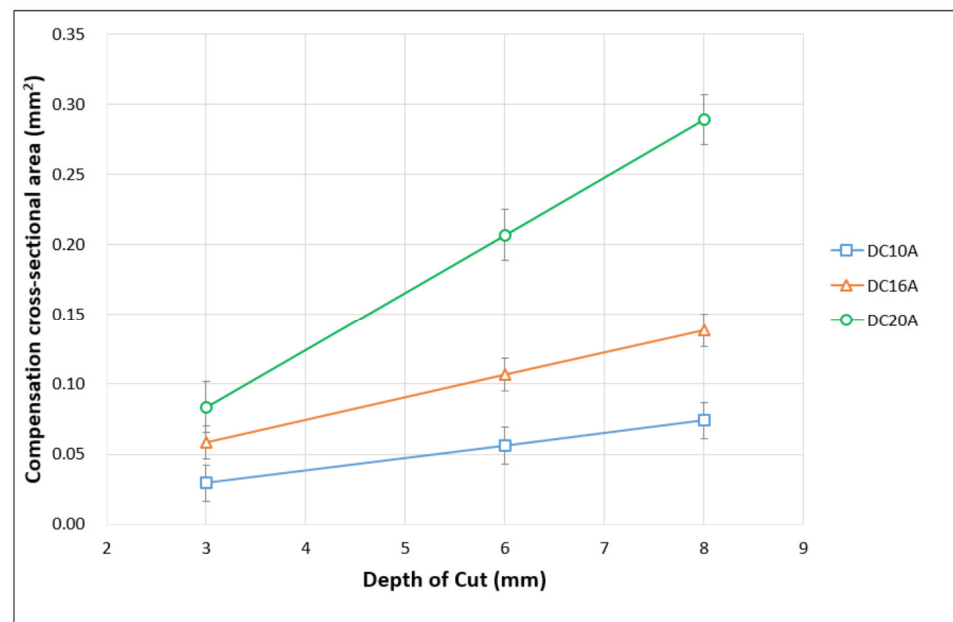


Figure 15. Electrode front-end protrusion cross-sectional area for electrode diameter 15 mm.

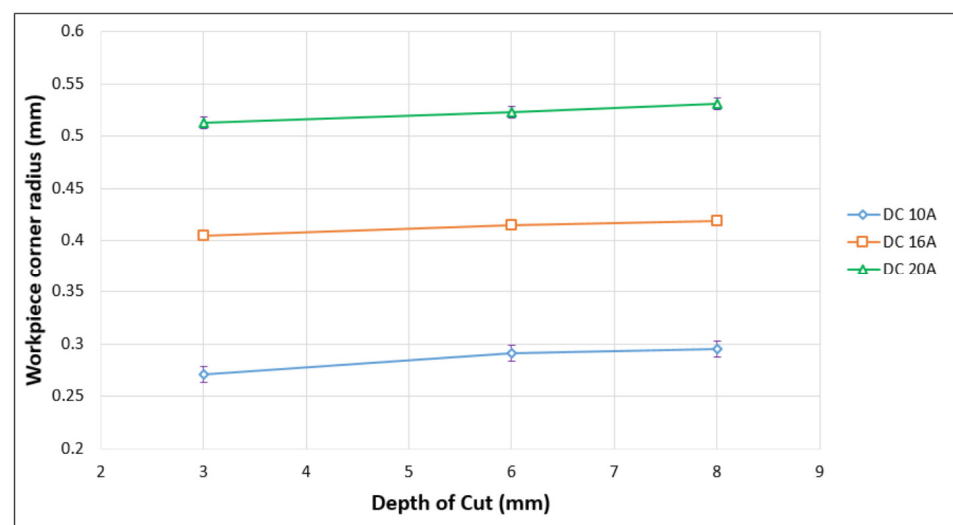


Figure 16. Verification result of workpiece corner radius with electrode diameter 10 mm.

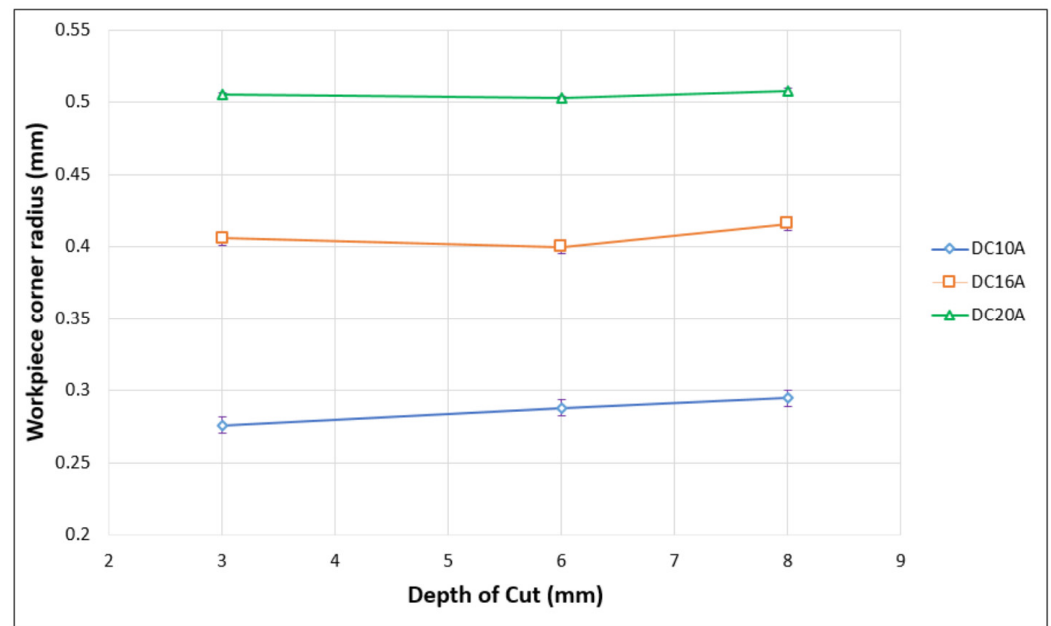


Figure 17. Verification result of workpiece corner radius with electrode diameter 15 mm.

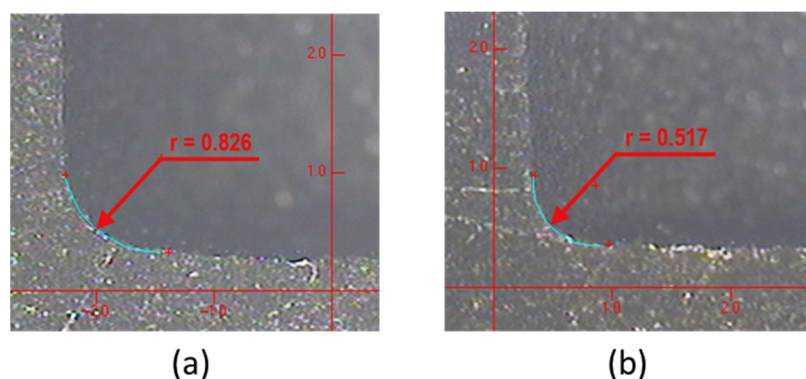
The second part of the verification experiment also carried out six experiments. The experiment conditions are presented in Table 11. The experiment results are shown in Table 12. It can be seen that the predicted and actual measurement of the workpiece corner radii for experiment #1 with cylinder electrodes are 0.825 and 0.826 mm. Meanwhile, the workpiece corner radii with the electrode front-end face design are 0.510 and 0.517 mm. The accuracy of the workpiece corner improves by 37.4%. Additionally, the prediction accuracy is 98.6%. Figure 18 shows the actual measurement of the workpiece corner radius with a cylinder electrode and the electrode front-end face design. As seen in Table 12, the deviation between the predicted and actual measurement value is within 10 μm , and the prediction accuracy is above 98% for all conditions except for verification experiment #4, in which the prediction error is 33 μm . This error might be due to the current density. When the discharge current is larger, the workpiece corner radius also becomes larger, but the influence of the machining depth on the workpiece corner is relatively small. As shown in Table 13 for different discharge currents, the workpiece corner becomes larger as the discharge current increases. The amount of discharge current determines the shape of the workpiece corner that is produced by electrode front-end face design. However, if the volume of the electrode front-end protrusion is too large, there is a circular pit defect, which results in poor accuracy.

Table 11. Machining condition of verification experiment.

Exp. Number	Electrode Diameter (mm)	Discharge Current (A)	Depth of Cut (mm)
#1	10	20	5
#2	10	20	10
#3	10	14	3
#4	10	8	6
#5	13	16	3
#6	8	16	3

Table 12. Verification result of predicted and actual measurement of workpiece corner radius.

Exp. Number	Workpiece Corner Radius	Cylinder Electrode (mm)			Electrode Front-End Face Design (mm)			Accuracy Improvement (%)
		Predicted by System	Actual Measurement	Errors (%)	Predicted by System	Actual Measurement	Errors (%)	
#1		0.825	0.826	0.13	0.510	0.517	1.35	37.4
#2		1.190	1.184	0.51	0.525	0.520	0.96	56
#3		0.439	0.437	0.46	0.369	0.370	0.27	15.3
#4		0.370	0.371	0.27	0.272	0.275	1.09	25.8
#5		0.519	0.523	0.77	0.409	0.412	0.72	21.2
#6		0.468	0.467	0.22	0.417	0.420	0.71	10

**Figure 18.** Actual measurement of workpiece corner radius with (a) cylinder electrode (b) electrode front-end face design.**Table 13.** Discharge current vs. workpiece corner radius.

Discharge Current (A)	Actual Measurement of Workpiece Corner Radius (mm)
8	0.275 ± 0.02
10	0.291 ± 0.02
16	0.415 ± 0.02
20	0.523 ± 0.02

6. Conclusions

In this study, an electrode front-end face design to improve the accuracy of workpiece corners was proposed. An experiment with different discharge currents, electrode diameters, and depth of cut was conducted. Three electrode front-end protrusion designs were proposed and used for the experiment. Multiple linear regression and ANOVA were used to analyze and investigate the effect of each parameter on the workpiece corner. The experiment results show that the discharge current has the most significant effect on the workpiece corner, followed by depth of cut and electrode diameter. Additionally, it is found that the volume of electrode wear is equal to the volume of workpiece corner, therefore, it can be used to design the electrode front-end face protrusion that compensates for the

workpiece corner. The experiment results demonstrate that width and height ratio of protrusion has a lesser effect on the workpiece corner accuracy.

Based on the experimental results, it is found that circular pit defects appear on the workpiece surface with a machining depth of 3 mm. This is because the electrode front-end protrusion volume is not completely consumed. Therefore, at a machining depth of 3 mm, the volume of the electrode front-end protrusion needs to be reduced to 50%, 85%, and 90% for discharge currents of 10, 16, and 20 A, respectively, to avoid the occurrence of circular pit defects on the workpiece surface.

A user-friendly human–machine interface that can predict the workpiece corner error and design electrode with compensation was built and tested. The verification experiments result show that the prediction accuracy can achieve 99.8%. The average prediction error is 0.81%. These results demonstrate that the proposed method and system can improve the accuracy of the workpiece corner. This study only used cylindrical-shaped electrodes. The various shapes of electrode, workpiece materials, and electrode materials are under investigation and will be published in the near future.

Author Contributions: Conceptualization, S.-M.W. and J.-K.P.; methodology, S.-M.W. and J.-K.P.; software, J.-K.P.; validation, J.-K.P. and H.G.; formal analysis, S.-M.W., J.-K.P. and H.G.; investigation, S.-M.W. and J.-K.P.; resources, S.-M.W. and J.-K.P.; data curation, J.-K.P., R.-Q.T., H.G. and S.-J.C.; writing—original draft preparation, S.-M.W. and H.G.; writing—review and editing, S.-M.W. and H.G.; visualization, J.-K.P., R.-Q.T., H.G. and S.-J.C.; supervision, S.-M.W. All authors have read and agreed to the published version of the manuscript.

Funding: This research was funded by National Science and Technology Council Taiwan, grant number MOST 111-2221-E-005 -080 -MY2, MOST 111-2218-E-005-010, and MOST 111-2218-E-005-011.

Data Availability Statement: Data sharing is not applicable to this article.

Conflicts of Interest: The authors declare no conflict of interest.

References

1. Gnanavel, C.; Saravanan, R.; Chandrasekaran, M.; Pugazhenth, R. Restructured review on electrical discharge machining—A state of the art. *IOP Conf. Ser. Mater. Sci. Eng.* **2017**, *183*, 012015. [[CrossRef](#)]
2. Prakash, V.; Kumar, P.; Singh, P.; Hussain, M.; Das, A.K.; Chattopadhyaya, S. Micro-electrical discharge machining of difficult-to-machine materials: A review. *Proc. Inst. Mech. Eng. Part B J. Eng. Manuf.* **2019**, *233*, 339–370. [[CrossRef](#)]
3. Papazoglou, E.L.; Karmiris-Obratanski, P.; Leszczynka-Madej, B.; Markopoulos, A.P. A study on electrical discharge machining of titanium grade2 with experimental and theoretical analysis. *Sci. Rep.* **2021**, *11*, 8971. [[CrossRef](#)] [[PubMed](#)]
4. Ishfaq, K.; Asad, M.; Anwar, S.; Pruncu, C.I.; Saleh, M.; Ahmad, S. A comprehensive analysis of the effect of graphene-based dielectric for sustainable electric discharge machining of Ti-6Al-4V. *Materials* **2021**, *14*, 23. [[CrossRef](#)] [[PubMed](#)]
5. Jain, S.; Parashar, V. Critical review on the impact of EDM process on biomedical materials. *Mater. Manuf. Process.* **2021**, *36*, 1701–1724. [[CrossRef](#)]
6. Boothroyd, G.; Winston, A.K. Non-conventional machining processes. In *Fundamentals of Machining and Machine Tools*; Marcel Dekker, Inc.: New York, NY, USA, 1989; p. 491.
7. Ho, K.H.; Newman, S.T. State of the Art Electrical Discharge Machining (EDM). *Int. J. Mach. Tools Manuf.* **2003**, *43*, 1287–1300. [[CrossRef](#)]
8. Nahak, B.; Gupta, A. A review on optimization of machining performance and recent development in electro discharge machining. *Manuf. Rev.* **2019**, *6*, 2. [[CrossRef](#)]
9. Das, S.; Paul, S.; Doloi, B. Assessment of the impact of bio-electrics on the textural features and recast-layer of EDM surfaces. *Mater. Manuf. Process.* **2020**, *36*, 245–255. [[CrossRef](#)]
10. Walia, A.S.; Srivasta, V.; Verma, K. Modelling of surface roughness and change in out-of-roughness of tool during electrical discharge machining with cermet tool tip using machine learning. *Processes* **2022**, *10*, 252. [[CrossRef](#)]
11. Beniak, J.; Krizan, P.; Soos, L.; Matus, M. Research on shape and dimensional accuracy of FDM produced parts. *IOP Conf. Ser. Mater. Sci. Eng.* **2019**, *501*, 012030. [[CrossRef](#)]
12. Bhosle, R.B.; Sharma, S.B. Multi-performance optimization of micro-EDM drilling process of Inconel 600 alloy. *Mater. Today Proc.* **2017**, *4*, 1988–1997. [[CrossRef](#)]
13. Cyril, J.; Paravasu, A.; Jerald, J.; Sumit, K.; Kanagaraj, G. Experimental investigation on performance of additive mixed dielectric during micro-electric discharge drilling on 316L stainless steel. *Mater. Manuf. Process.* **2017**, *32*, 638–644. [[CrossRef](#)]
14. Batish, A.; Bhattacharya, A.; Kumar, N. Powder mixed dielectric: An approach for improved process performance in EDM. *Part. Sci. Technol.* **2015**, *33*, 150–158. [[CrossRef](#)]

15. Zainal, N.; Zain, A.M.; Sharif, S.; Hamed, H.N.A. A study of dimensional accuracy on die sinking electrical discharge machining of Ti-6Al-4V. *Indian J. Sci. Technol.* **2017**, *10*, 1–6. [[CrossRef](#)]
16. Anand, B.; Giri, A.; Mohanty, C.P.; Sharma, D. Tool wear and energy consumption optimization in EDM of Chromium tool steel. *Mater. Today Proc.* **2021**, *43*, 268–272. [[CrossRef](#)]
17. Ahmed, N.; Anwar, S.; Ishfaq, K.; Razaqat, M.; Saleh, M.; Ahmad, S. The potentiality of sinking EDM for micro-impressions on Ti-6AL-4V: Keeping the geometrical errors (axial and radial) and other machining measures (tool erosion and work roughness) at minimum. *Sci. Rep.* **2019**, *9*, 17218. [[CrossRef](#)]
18. Mandal, D.; Pal, S.K.; Saha, P. Back propagation neural network based modeling of multi-responses of an electrical discharge machining process. *Int. J. Knowl. Based Intell. Eng. Syst.* **2007**, *11*, 381–390. [[CrossRef](#)]
19. Muthuramalingam, T.; Mohan, B. Influence of tool electrode properties on machinability in spark erosion machining. *Mater. Manuf. Process.* **2013**, *28*, 939–943. [[CrossRef](#)]
20. Muthuramalingam, T.; Mohan, B.; Jothilingam, A. Effect of tool electrode resolidification on surface hardness in electrical discharge machining. *Mater. Manuf. Process.* **2014**, *29*, 1374–1380. [[CrossRef](#)]
21. Prasanna, J.; Rajamanickam, S. Investigation of die sinking electrical discharge machining of Ti-6Al-4V using copper and Al₂O₃-TiO₂ coated copper electrode. *Middle-East J. Sci. Res.* **2016**, *24*, 33–37.
22. Karmiris-Obratanski, P.; Zagorski, K.; Papazoglou, E.L.; Karkalos, N.E.; Markopoulos, A.P. On machining Ti6Al4V ELI with EDM by using copper and graphite electrodes: A comparison study. *IOP Conf. Ser. Mater. Sci. Eng.* **2021**, *1037*, 012003. [[CrossRef](#)]
23. Ishfaq, K.; Farooq, M.U.; Pruncu, C.I. Reducing the geometrical machining errors incurred during die repair and maintenance through electric discharge machining (EDM). *Int. J. Adv. Manuf. Technol.* **2021**, *117*, 3153–3168. [[CrossRef](#)]
24. Mufti, N.A.; Razaqat, M.; Ahmed, N.; Saleem, M.Q.; Hussain, A.; Al-Ahamri, A.M. Improving the performance of EDM through relief-angled tool design. *Appl. Sci.* **2020**, *10*, 2432. [[CrossRef](#)]
25. Liang, W.; Tong, H.; Li, Y.; Li, B. Tool electrode wear compensation in block divided EDM process for improving accuracy of diffuser shape film cooling holes. *Int. J. Adv. Manuf. Technol.* **2019**, *103*, 1759–1767. [[CrossRef](#)]
26. Lo, J.S.; Jiang, C.T. Compensation method for profile deviations caused by the complex shape of electrodes in orbital electrical discharge machining. *Int. J. Adv. Manuf. Technol.* **2019**, *103*, 841–848. [[CrossRef](#)]
27. Richard, J.; Giandomenico, N. Electrode profile prediction and wear compensation in EDM-milling and micro-EDM-milling. In Proceedings of the 19th CIRP Conference on Electro Physical and Chemical Machining, Bilbao, Spain, 23–27 April 2018.
28. Pei, J.; Zhuang, X.; Zhang, L.; Zhu, Y.; Liu, Y. An improved fix-length compensation method for electrical discharge milling using tubular tool. *Int. J. Mach. Tools Manuf.* **2018**, *124*, 22–32. [[CrossRef](#)]
29. Yu, H.L.; Luan, J.J.; Li, J.Z.; Zhang, Y.S.; Yu, Z.Y.; Guo, D.M. A new electrode wear compensation method for improving performance in 3D micro EDM milling. *J. Micromech. Microeng.* **2010**, *20*, 055011. [[CrossRef](#)]
30. Pham, D.T.; Dimov, S.S.; Bigot, S.; Ivanov, A.; Popov, K. Micro EDM recent developments and research issues. *J. Mater. Process. Technol.* **2004**, *149*, 50–57. [[CrossRef](#)]
31. Singh, H. Investigating the effect of copper chromium and aluminum electrodes on EN-31 die steel on dielectric discharge machine using positive polarity. In Proceedings of the World Congress on Engineering, London, UK, 4–6 July 2012.
32. Wang, S.M.; Wu, J.X.; Gunawan, H.; Tu, R.Q. Optimization of machining parameters for corner accuracy improvement for WEDM processing. *Appl. Sci.* **2022**, *12*, 10324. [[CrossRef](#)]

Disclaimer/Publisher’s Note: The statements, opinions and data contained in all publications are solely those of the individual author(s) and contributor(s) and not of MDPI and/or the editor(s). MDPI and/or the editor(s) disclaim responsibility for any injury to people or property resulting from any ideas, methods, instructions or products referred to in the content.